Bioprinting 28 (2022) e00229

Contents lists available at ScienceDirect

Bioprinting

journal homepage: www.sciencedirect.com/journal/bioprinting

Automated and dynamic extrusion pressure adjustment based on real-time flow rate measurements for precise ink dispensing in 3D bioprinting

Lukas Wenger [a,1], Svenja Strauß [b,1], Jürgen Hubbuch [a,b,*]

[a] Institute of Process Engineering in Life Sciences, Section IV: Biomolecular Separation Engineering, Karlsruhe Institute of Technology, Fritz-Haber-Weg 2, 76131, Karlsruhe, Germany
[b] Institute of Functional Interfaces, Karlsruhe Institute of Technology, Hermann-von-Helmholtz-Platz 1, 76344, Eggenstein-Leopoldshafen, Germany

ARTICLE INFO

Keywords:
3D printing
Bioprinting
Bioink
Hydrogels
Liquid flow meter
Process control
Adaptive pressure control
Flow regulation

ABSTRACT

Extrusion-based printing relying on pneumatic dispensing systems is the most widely employed tool in bioprinting. However, standardized and reliable methods for process development, monitoring and control are still not established. Suitable printing parameters are often determined in a trial-and-error approach and neither process monitoring nor real-time adjustments of extrusion pressure to environmental and process-related changes are commonly employed. The present study evaluates an approach to introduce flow rate as a main process parameter to monitor and control extrusion-based bioprinting. An experimental setup was established by integrating a liquid flow meter between the cartridge and nozzle of a pneumatically driven bioprinter to measure the actual flow of dispensed ink in real-time. The measured flow rate was fed to a Python-based software tool implementing a proportional-integral-derivative (PID) feedback loop that automatically and dynamically adapted the extrusion pressure of the bioprinter to meet a specified target flow rate. The performance of the employed experimental setup was evaluated with three different model inks in three application examples. a) Continuous dispensing: Several runs of continuous dispensing showed that the PID-based pressure control was able to generate a steady flow rate more consistently and precisely than constant pressure settings. b) Adaptation to ink inhomogeneities: Deliberately created ink inhomogeneities were successfully compensated for by real-time pressure adjustments which profoundly enhanced the printing quality compared to printing without adaptive pressure. c) Process transfer to other nozzle types: Experiments with different nozzle types demonstrated the potential of the established setup to facilitate and accelerate process transfer and development. The present study provides an alternative approach for process design, monitoring and control by introducing flow rate as a main process parameter. We propose bioprinting processes to be based on flow rate specifications instead of constant pressure settings. This approach has the potential to save time by avoiding tedious parameter screenings and to introduce an active, real-time control over the printing process. Subjective influences by individual users during process development can be reduced and the process transfer between different devices and experimental setups can be facilitated and accelerated.

1. Introduction

Additive manufacturing, or 3D printing, is a collective term for a variety of fabrication techniques to produce three-dimensional objects by gradually adding material in a layer-by-layer buildup process [1]. 3D printing is already established in areas like mechanical engineering and the aerospace industry and is increasingly spreading into other fields like biotechnology [2–5]. Novel applications in disciplines such as tissue engineering [6], smart materials [7] or bioprocess engineering [8,9] already show the potential of this technique. Tissue engineering aims at designing artificially made and functional substitutes to restore, maintain or support the function of natural tissues [10]. The fabrication of such substitutes requires the embedding of living cells within a supporting matrix material mimicking the natural environment of living tissue [11]. Hydrogels are typically chosen for that purpose due to their aqueous nature and high biocompatibility [11]. Another common

* Corresponding author. Institute of Process Engineering in Life Sciences, Section IV: Biomolecular Separation Engineering, Karlsruhe Institute of Technology, Fritz-Haber-Weg 2, 76131, Karlsruhe, Germany.
E-mail address: juergen.hubbuch@kit.edu (J. Hubbuch).
[1] Contributed equally.

https://doi.org/10.1016/j.bprint.2022.e00229
Received 25 April 2022; Received in revised form 24 June 2022; Accepted 18 July 2022
Available online 30 July 2022

application for hydrogels is the immobilization of enzymes by physical entrapment [12]. Hydrogels or hydrogel precursor solutions are often employed in bioprinting, an interdisciplinary field combining 3D printing and biofabrication with the objective to print biologically functional constructs like living tissues [13]. In this context, the hydrogel precursor solutions are typically referred to as *bioinks* when containing living cells, or as *biomaterial inks* if they are cell-free [14]. Depending on the field of application and the printing method, bioinks need to meet certain criteria like cytocompatibility, specific rheological properties and the ability for crosslinking [13]. To meet these requirements, bioinks are often hybrid materials containing several components like polymers, rheological additives and crosslinkable components. The polymers can be synthetic, e. g. based on polyethylene glycol (PEG) or poloxamer, or naturally derived, e. g. based on agarose, alginate, chitosan, hyaluronic acid, fibrin, or collagen. Depending on the intended use, the polymers can be chemically modified and, for example, ligands for cell adhesion can be incorporated. The polymers can be crosslinked physically, chemically, thermally, enzymatically or by photopolymerization [15,16]. Certain hydrogels, e. g. based on poloxamer, are also used as a sacrificial support material that is removed after printing [17].

In bioprinting, a variety of methods like inkjet-, laser- or stereolithography-based bioprinting is available. The most common method, especially in cell-based printing, is extrusion-based bioprinting (EBB) [13] which relies on a steady flow of material being dispensed from a cartridge. EBB methods can be classified by the employed dispensing system which can be based on pneumatic or mechanical extrusion, with each method having different advantages and disadvantages [6,13]. Pneumatic systems use pressurized air to extrude material, while mechanical systems are driven by a piston or a screw [13]. Piston-based systems theoretically allow a more precise control of the extruded volume as the flow rate is directly correlated to the movement of the piston and the cartridge dimensions. The flow rate can be set independently of the material by defining the piston speed, but there is a tendency of lagging leakage at the end of an extrusion process which can be counteracted by retracting the piston or adding a valve [18,19]. Screw-based systems allow excellent control of the extruded volume, but cleaning the system is tedious and often accompanied by a high loss of material due to dead volume [20]. This may be problematic when working with costly bioinks and slowly growing cells. The screw-driven mechanism induces higher shear forces which can result in increased cell damage, depending on the design of the screw and the printing conditions [21].

Pneumatic dispensing is widely employed due to its simplicity [6], but it is prone to delays due to the compression of gas volume within the cartridge which can reduce the printing precision [16,22]. In pneumatic dispensing systems, the resulting flow rate cannot be controlled directly, as it is not only dependent on the applied pressure, but also on the rheological properties of the bioink and the components of the experimental setup like the nozzle. This makes the method susceptible to unintended variations of the experimental conditions. Therefore, environment-related parameters like temperature or humidity, system-related parameters like cartridge fill level, or material-related parameters, such as inhomogeneities or batch-to-batch variations of the bioinks, can have a relevant effect on the generated flow rate and hence the outcome of the printing process [23–27]. Compensating for such variations may require a change in extrusion pressure to achieve the desired flow rate. However, the most common approach to bioprinting process development is to define constant printing parameters or working windows either systematically or by trial and error [24,27,28]. These approaches are usually based on indirect parameters like rheological properties of inks [24] or qualitative aspects like filament formation [29]. Other methods include the analysis of strand widths [30] or filament fusion [27] by structural image analysis. In order to handle variations of bioink properties or environmental conditions, all these approaches may require parameter screenings before performing a printing run, depending on the robustness of the process. An alternative approach is to reduce the environmental variations to a minimum by placing the bioprinter in a temperature- and humidity-controlled environment [31]. However, both strategies cannot equally handle both batch-to-batch variations of the bioink and time-dependent environmental changes.

Direct real-time monitoring of bioprinting processes is relatively uncommon, but previous studies have shown that liquid flow sensors can be employed to monitor the flow rate during bioprinting and to observe batch- and time-related changes in the relation of pressure and flow [32,33]. Flow sensors are currently used for industrial applications in the automotive, oil and gas industry, but also in the food and beverage and pharmaceutical industry [34–40]. A range of different flow sensors are available which can be classified based on the employed measurement principle. Thermal flow sensors derive the flow rate from the travel time of heat pulses or the temperature profile around a heater [41]. Non-thermal sensors are based on other physical principles [41]. Today, very small flow meters can be produced with many advantages such as a lack of moving parts, better dynamic characteristics, low power consumption, low cost and easier integration into other systems [42]. Progress in the production of microelectromechanical systems allowed the development of micromachined thermal flow sensors which can be applied in the medical field to monitor blood and respiratory flow or drug delivery [38,43,44].

While it has been shown that flow sensors can be employed in bioprinting for process monitoring [33], there is still no demonstration of how to use the flow data obtained during extrusion in order to dynamically adapt the pressure and create a steady flow, independent of interference factors like temperature, cartridge fill level and other parameters. The present work introduces an experimental setup including a liquid flow sensor as a part of a feedback-loop controlling the pressure of a pneumatically driven bioprinter. A Python-based software tool is developed to read and record the sensor data and to generate a steady flow rate by continuously adapting the pressure based on a proportional-integral-derivative (PID)-controlled feedback loop. The developed setup is tested with three different model inks, two of which are based on the synthetic polymer poloxamer 407 (also known as Pluronic® F-127 or Kolliphor® P407) in different concentrations. Poloxamer 407 inks are suitable model inks due to their excellent printability and simple preparation [17,24,45]. Additionally, an ink based on the natural polymer alginate and the additive Laponite® RD is investigated. Alginate is a very common component of bioinks due to its gelling properties [46–49] and Laponite® RD is typically employed as an inorganic filler to increase viscosity and enhance printability [8,50,51]. The performance of the employed adaptive pressure control setup was investigated in three application examples. a) Continuous dispensing: The general behavior of the flow sensor and the ability of the PID control to generate a constant flow were tested using continuous dispensing runs. b) Adaptation to ink inhomogeneities: The suitability for realistic printing applications was tested by printing from a cartridge with an intentionally inhomogeneous ink created by alternating layers of poloxamer 407 inks of different concentrations. c) Process transfer to other nozzle types: As an example for process transfer, the ability of the setup to adapt to different nozzle types was tested. An overview of the employed workflow is depicted in Fig. 1.

2. Materials and methods

2.1. Ink preparation

Sodium alginate and poloxamer 407 were both obtained from Sigma Aldrich (St. Louis, USA) and Laponite® RD from BYK-Chemie GmbH (Wesel, Germany). Three different inks were prepared by dissolving the appropriate amounts of the respective components in ultrapure water (arium® pro VF, Satorius AG, Göttingen, Germany) and mixing at 3500 rpm in a SpeedMixer® (Hauschild GmbH & Co. KG, Hamm, Germany),

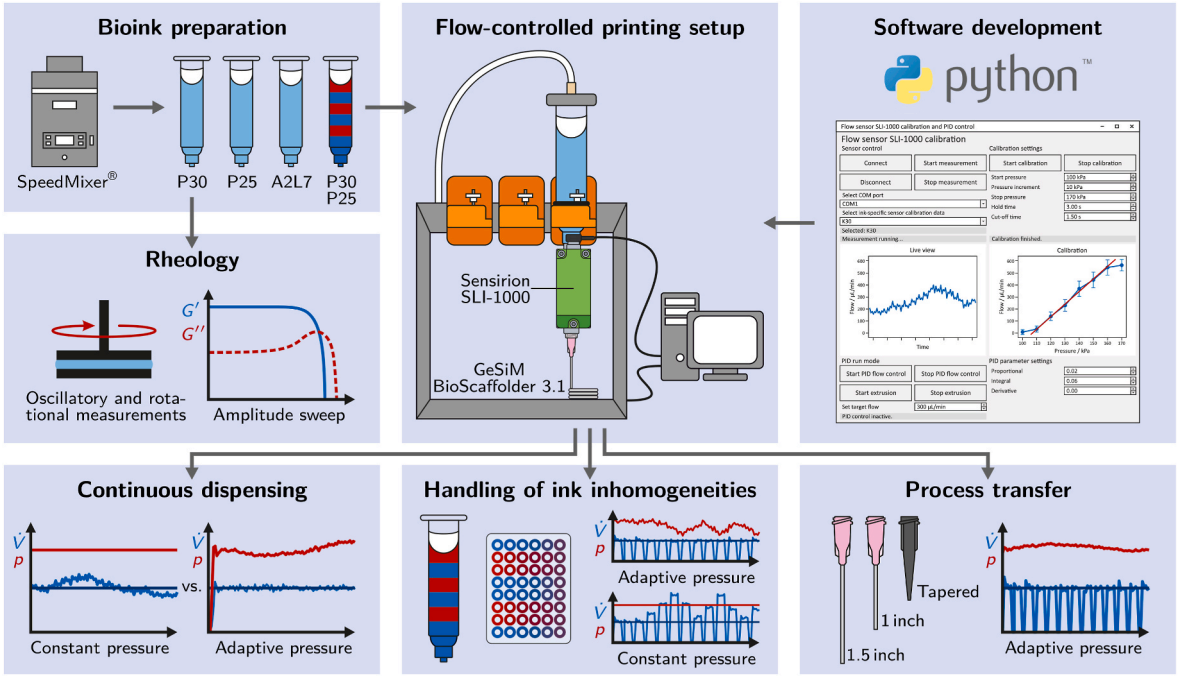

Fig. 1. Schematic of the workflow applied in the present study. Three different inks are prepared and analyzed with rheological methods. A Python-based software tool is developed that implements a PID control loop to continuously adapt the extrusion pressure of a pneumatic bioprinter based on real-time data from a liquid flow meter. The integrated PID control setup is evaluated in three separate application examples.

until a homogenous mixture was obtained. Poloxamer-based inks were cooled in an ice bath between mixing steps to increase solubility. Three different ink compositions were prepared, the first one containing 30% (w/w) poloxamer 407 (P30), the second one 25% (w/w) poloxamer 407 (P25) and the third one 2% (w/w) sodium alginate with 7% (w/w) Laponite® RD (A2L7). An overview of the employed inks and their components is given in Table 1. The prepared inks were filled into 10 mL cartridges (Nordson Corporation Westlake, USA) and centrifuged at 600 g for 10 min to minimize the amount of entrapped air bubbles. The cartridges were sealed with pneumatic pistons (Nordson Corporation Westlake, USA) for printing.

2.2. Rheology

The rheological behavior of P30, P25, and A2L7 was investigated using the rheometer Physica MCR301 (Anton Paar GmbH, Graz, Austria). A setup with parallel stainless steel plates with a diameter of 25 mm was employed for all rheological experiments. The gap width was 150 µm and all measurements were performed at 20 °C as technical triplicates ($n = 3$).

Yield stress values were determined from shear stress-controlled rotational tests. The deformation was plotted against shear stress on a logarithmic scale. The yield stress was determined by fitting the two linear regions of the plot with tangents and calculating the shear stress at their point of intersection.

Oscillatory measurements were performed with controlled shear stress τ in a range of 1–1000 Pa at an angular frequency of $\omega = 10\ s^{-1}$. For each measurement, the loss factor $\tan\delta = G''/G'$ was determined by averaging G' and G'' in the region from $\tau = 10$ Pa to $\tau = 100$ Pa which was within the linear viscoelastic (LVE) region and low in noise for each measurement.

Table 1
Ink compositions with the corresponding extrusion pressure, as employed for printing runs with a constant pressure setting. The pressure was determined from the first adaptive dispensing run with a 1 inch nozzle and a target flow rate of 300 µL/min by averaging the applied pressure over a period of 10 min.

Abbreviation	Poloxamer 407	Alginate	Laponite® RD	Extrusion pressure
	(% (w/w))	(% (w/w))	(% (w/w))	(kPa)
P30	30	–	–	436
P25	25	–	–	256
A2L7	–	2	7	329

2.3. Adaptive PID pressure control: hardware and software setup

The main objective of the present study was to establish a tool that enables flow-based process control for pneumatic extrusion-based bioprinting. The approach was to employ a software-based proportional-integral-derivative (PID) control that uses input data from a liquid flow meter to adapt the extrusion pressure of a pneumatic bioprinter in real-time. The components of the established setup and their interactions are described in the following sections.

2.3.1. Hardware configuration

All conducted dispensing and printing experiments were performed on a BioScaffolder 3.1 bioprinter (GeSiM mbH, Radeberg, Germany) with three pneumatic extrusion heads. An SLI-1000 liquid flow meter (Sensirion, Stäfa, Switzerland) was employed to measure the flow rate of inks during printing. The SLI-1000 contains a straight glass capillary with an inner diameter of 1 mm and is specified for flow rates up to 1000 µL/min with water. The sensor relies on calorimetric sensing, a measurement principle that derives flow rates from thermal profiles forming around a heating element depending on the current fluid flow [42]. In the case of the Sensirion SLI-1000, two thermal sensors are placed up- and downstream of the heating element to detect the thermal profile, as indicated in Fig. 2A. The flow sensor was attached below one of the extrusion heads of the BioScaffolder using a customized, 3D-printed mount. A USB cable enabled the communication between flow sensor and computer via RS485 interface.

The arrangement of the components allowed a cartridge to be directly attached to the inlet on the upper side of the liquid flow meter

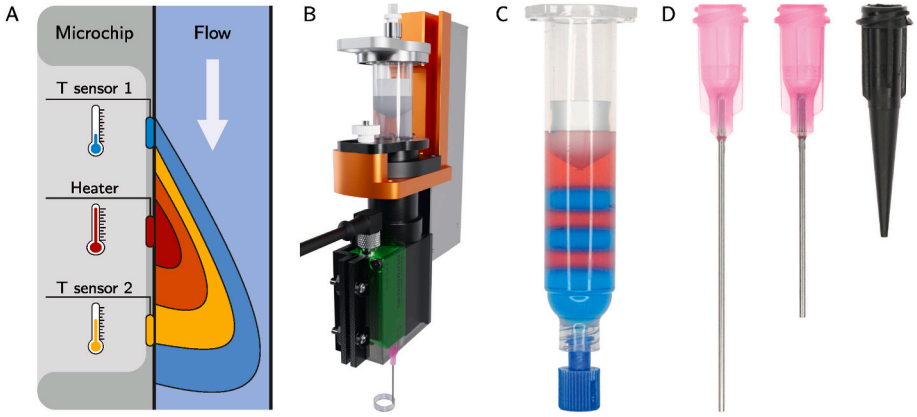

Fig. 2. (A) Schematic representation of the thermal measuring principle of the liquid flow meter. Adapted from Schnell et al. [52] and Kuo et al. [42]. (B) 3D visualization of the arrangement of the hardware components of the PID control setup. The sensor is attached below the extrusion head of the bioprinter using a 3D-printed mount. The right part of the mount is shown as transparent to reveal the flow sensor. A cartridge is connected to the sensor inlet on the top, a nozzle to the outlet at the bottom. The CAD file of the sensor was obtained from Sensirion [53]. (C) Printer cartridge filled with alternating layers of P30 (blue) and P25 (red). The layered material served as a performance test for the PID-controlled printing setup. (D) Dispensing tips used in this study, from left to right: 1.5 inch straight nozzle, 1 inch straight nozzle, tapered nozzle. All nozzles had an orifice diameter of 0.58 mm. Depending on length and geometry, even dispensing tips with identical orifice diameter can generate massively different back pressures. (For interpretation of the references to color in this figure legend, the reader is referred to the Web version of this article.)

and a nozzle to the outlet at the bottom side. The setup reduced the amount of available space in the z-direction, but otherwise enabled unrestricted printing. Fig. 2B shows the employed setup while printing a hollow cylinder.

2.3.2. *Software development*

A software tool based on Python 3.8.5 (Python Software Foundation, Delaware, USA) was developed to integrate the liquid flow meter and the pneumatic extrusion bioprinter into a PID-controlled feedback loop that constantly adapts the extrusion pressure to keep the resulting ink flow at a constant target value. A scheme representing all the components involved in the PID control and their interactions is shown in Fig. 3. In short, the user sets the target flow rate and PID parameters using a graphical user interface (GUI). The Python-based software receives real-time data from the liquid flow meter which is converted to flow rate values using imported calibration curves. To generate the desired target flow rate, the software-based PID control constantly adapts the pressure by sending commands to the GeSiM Robotics software which controls the GeSiM BioScaffolder. The flow rate data and pressure settings are stored and exported for later evaluation.

2.3.2.1. Graphic user interface. For easy interaction with the user, a graphical user interface (GUI) was developed that allowed controlling the flow sensor, performing calibrations and adjusting the PID control. Fig. 4 shows the GUI of the developed Python tool with the GUI of the GeSiM Robotics software in the background. The GUI was split in several sections. The top left section provided the flow sensor control panel including buttons to connect and disconnect and to start and stop measurements. The COM port of the flow sensor and the appropriate ink calibration could be selected from drop-down menus. Depending on the selection, the ink-specific calibration data necessary to convert the sensor output to flow values were loaded from an external Excel file. Section 2.4.1 describes how the calibration data were generated using a syringe pump and an adapted version of the Python tool. Below the sensor control panel, the GUI showed a graph with a live view of the current flow measurement.

Another control panel to perform pressure-flow calibrations was located in the top right part of the GUI, accompanied by an additional graph showing the determined calibration points with the respective calibration curve. This feature allowed determining the correlation between applied pressure and resulting flow rate for a specific ink and experimental setup. Within the scope of this paper, this feature was not applied but it may be used to characterize the flow behavior of inks under certain conditions. The bottom part of the GUI accommodated the PID control panel including buttons to start and stop the PID control and the extrusion process. Input fields allowed setting the target flow rate and the PID parameters.

2.3.2.2. Device communication. Communication between the Sensirion SLI-1000 liquid flow meter and Python could be established by customizing code provided by Sensirion. The code was based on the *pySerial* package (version 3.5) which enables communication over the serial port. While running, the software constantly read out the current flow from the liquid flow meter at a rate of roughly five readings per second. During printing processes, the pressure is frequently turned on and off when switching from one strand or layer to the next. These

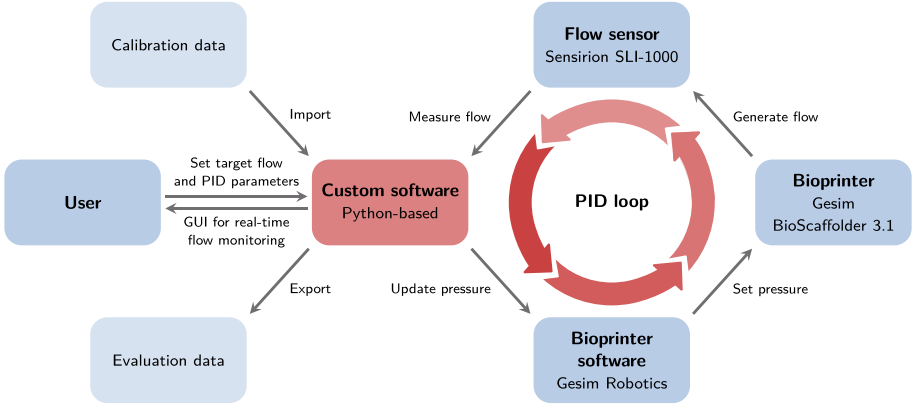

Fig. 3. Schematic of the interactions between the relevant components of the PID control setup.

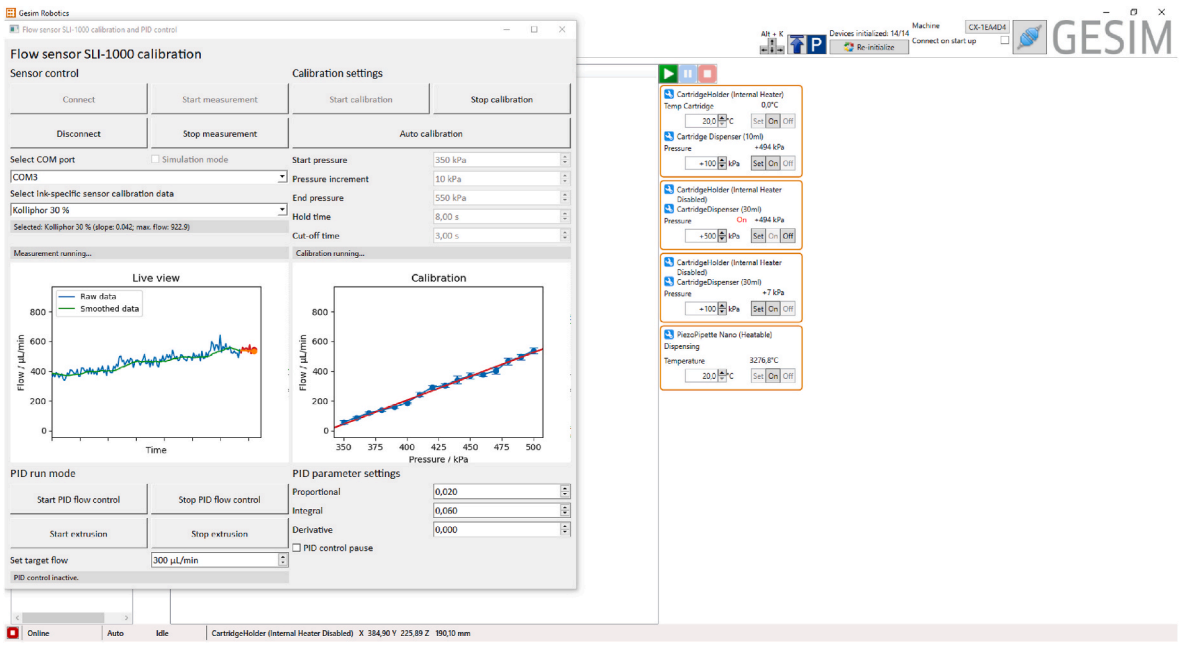

Fig. 4. Screenshot of the graphical user interface of the Python-based PID control tool. The example shows the calibration of the ink P30. The left graph represents a live view of the flow measurement data, the right graph shows data points obtained during the calibration. The GeSiM Robotics software being automatically operated by the Python tool is visible in the background.

switching operations are accompanied by a drop in flow rate that is irrelevant to the PID control. To ignore these irrelevant data points, only flow rate values larger than 3% of the sensor output limit were regarded as valid. To ignore spikes in flow rate that sometimes occurred with the switching operations, all data points deviating from the previous data point by more than 20% relative to the sensor output limit were regarded as invalid. Besides the raw flow rate data, an additional curve with smoothed data was plotted in the live view of the GUI. The smoothed data was obtained by determining a rolling average over the last 15 valid data points.

Direct communication between Python and the BioScaffolder 3.1 allowing real-time changes in pressure could not be established. As a workaround, the GeSiM Robotics software controlling the BioScaffolder was automatically operated by Python to trigger pressure changes. For this purpose, the *PyAutoGUI* package (version 0.9.52) was employed that allows performing automated operations on third-party GUIs like clicking buttons or entering text into input fields. This workaround allowed controlling the extrusion pressure of the BioScaffolder indirectly via Python, even during an active printing process.

2.3.2.3. PID-based pressure control. The software-based PID control loop was implemented in Python using the package *simple-pid* (version 0.2.4). In the active state, the PID loop was fed every 0.25 s with the last valid data point and the pressure in the Gesim Robotics software was updated every 0.5 s based on the output of the PID loop. Suitable PID control parameters (proportional, integral and derivative gain) were determined iteratively by trial-and-error and kept constant for all performed experiments, as shown in Table 2.

Table 2
Proportional, integral and derivative gain, as applied for all experiments involving the PID control for automatic pressure adjustment.

Gain parameter	Value
K_p (proportional)	0.02
K_i (integral)	0.06
K_d (derivative)	0.00

The applied PID algorithm of the *simple-pid* package is based on the controller output function

$$u(t) = K_p e(t) + K_i \int_0^t e(t)dt + K_d \frac{de(t)}{dt} \quad (1)$$

with the gain parameters K_p (proportional), K_i (integral) and K_d (derivative) and the error term

$$e(t) = r(t) - y(t) \quad (2)$$

where $r(t)$ is the reference input and $y(t)$ is the process variable [54,55]. In the given case, $u(t)$ is used as an input variable for the printer to set the current extrusion pressure, $r(t)$ is the set point of the flow rate for the PID control and $y(t)$ is the flow rate measured by the flow sensor. The integration of the PID controller within the experimental setup and the interaction between the components and their respective input and output variables is schematically shown in Fig. 5.

2.4. Application of the adaptive pressure control

2.4.1. Flow sensor calibration

The employed liquid flow meter SLI-1000 determines flow rates indirectly from heat distribution profiles within the fluid [56]. As such, it is substantially influenced by the specific thermal conductivity properties of the specific fluid [42] and requires individual calibrations when working with a variety of inks. Accordingly, calibration curves were determined for P30, P25 and A2L7 that allowed converting the sensor output data to flow rate values. To generate a defined volumetric flow rate through the SLI-1000 liquid flow meter, a Nemesys 290 N syringe pump with a 10 mL syringe (both Cetoni GmbH, Korbuβen, Germany) was employed. A slightly adapted version of the described Python software tool was applied to record the output data of the sensor and to adjust the syringe pump to different flow rates by operating the control software of the syringe pump (QmixElements, version 20140605). A screenshot of the software tool and the QmixElements software is shown in the supplementary material. Data points for the calibration curves were determined by setting a fixed flow rate for 30 s and determining the mean value of the sensor output of the last 20 s of this period. The flow

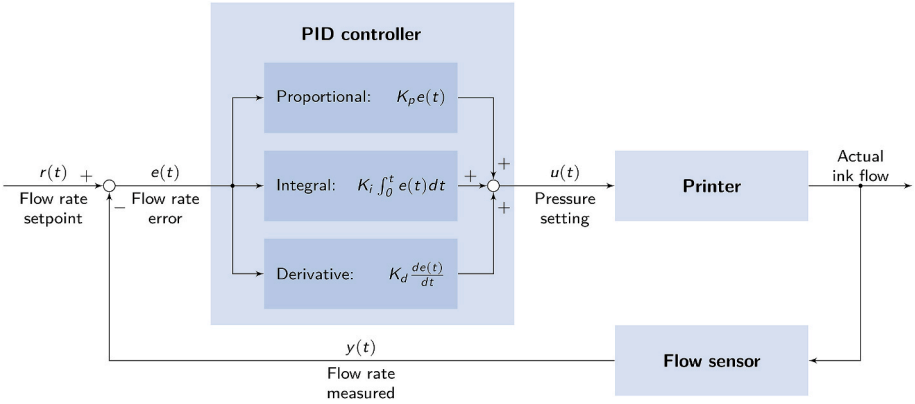

Fig. 5. Schematic block diagram of the employed PID feedback loop showing the interaction between printer, flow sensor and PID controller in combination with the respective input and output variables. Scheme adapted from Refs. [54,55].

rate was increased step-wise, until the sensor output limit was reached. The obtained data points were fitted with a linear equation. The resulting calibration curves are shown in the supplementary material and the equation parameters were stored in an Excel file that served as an input for the Python-based PID software tool.

2.4.2. Continuous dispensing

Continuous dispensing runs were performed as an initial performance test of the adaptive pressure control. For each ink, three runs were carried out with active PID control and three runs with a constant pressure setting ($n = 3$). Ink was dispensed from a 10 mL cartridge continuously for 30 min through a 1 inch straight nozzle with an inner orifice diameter of 0.58 mm (Vieweg GmbH, Kranzberg, Germany, see Fig. 2D). During the runs with adaptive pressure, a target flow rate of 300 µL/min was specified and the pressure was continuously adapted by the Python-based PID control tool described in Section 2.3.2. The applied pressure of the first run with adaptive pressure control was averaged over a period of 10 min and used as the pressure setting of the runs with constant pressure. The obtained constant pressure settings are presented in Table 1.

2.4.3. Adaptation to ink inhomogeneities

To verify the capability of the PID control to generate a constant flow independent of changing rheological properties of the ink, two cartridges were filled with alternating layers of P30 and P25. In order to highlight the different layers optically, P30 was spiked with blue and P25 with red food coloring. Before the cartridge was filled, the inks were liquefied by cooling to allow the handling with pipettes. After addition to the cartridge, each layer was allowed to solidify at room temperature, before the next layer was added. At the bottom of the cartridge was a layer of 2 ml P30, followed by 4 alternating 1 ml layers of P25 and P30, and at the top was a 2 ml layer of P25. A photograph of one of the cartridges is shown in Fig. 2C.

Hollow cylinders with a diameter of 10 mm and a height of 3 mm were printed as simple test objects onto a glass plate heated to 35 °C to avoid ink spreading. The layer height of the cylinders was 300 µm and the printing speed 10 mm/s. All prints were carried out with a straight 1 inch nozzle with an inner orifice diameter of 0.58 mm. One cartridge was used for each printing run. To evaluate the performance of the adaptive pressure control, the first run was performed with active adaptive pressure control and a target flow rate of 300 µL/min. Before starting the printing process, the adaptive pressure control was run for 30–60 s, until a constant flow was reached. The second printing was carried out with a constant pressure of 436 kPa which was determined to be suitable for P30 during the continuous dispensing runs (see Table 1).

2.4.4. Process transfer to other nozzle types

To investigate whether a flow rate-based process control facilitates the process transfer between different nozzle types, additional prints of hollow cylinders were carried out with the already employed 1 inch straight nozzle, a 1.5 inch straight nozzle and a tapered nozzle, all with an inner orifice diameter of 0.58 mm and obtained from Vieweg GmbH. The three nozzle types are depicted in Fig. 2D. Again, runs with adaptive pressure control were compared to runs with fixed extrusion pressure. With every run, two 3 mm high cylinders with a diameter of 10 mm and a layer height of 300 µm were printed at a speed of 10 mm/s on a plate heated to 35 °C. Before the runs with adaptive pressure control, the target flow rate was set to 300 µL/min and the adaptive pressure control was run for 30–60 s, until a constant flow was reached. The runs with constant pressure setting were carried out with the pressure that was determined to be suitable for the respective ink in combination with the 1 inch straight nozzle during the continuous dispensing runs (see Table 1).

3. Results and discussion

3.1. Implementation of the experimental setup

As the application of flow sensors is not an established practice in 3D bioprinting, a customized setup was designed to implement a Sensirion SLI-1000 liquid flow meter on a GeSiM BioScaffolder 3.1 bioprinter. As shown in Fig. 2B, the flow sensor was attached between the cartridge and the nozzle using a 3D-printed mount which allowed fast and easy assembly. However, the arrangement added a certain amount of complexity and some disadvantages to the experimental setup. The height of the sensor of 53 mm caused a reduction of available space in the z-direction despite the cartridge being mounted above its default location. The capillary of the sensor and the required Luer lock adapters added some dead volume which may be problematic when working with costly bioinks and sterile operation of the setup was made more difficult. These disadvantages can largely be attributed to the lack of optimization of the established setup. The employed flow sensor was neither optimized for the use with hydrogels, nor for the interoperability with a bioprinter. A more wide-spread application of flow sensors in bioprinting would require targeted adaptations like a reduction in size and cost. Smaller sensors with Luer locks would reduce both space requirements and dead volumes. Lower cost could enable the use of flow sensors as disposable products to simplify sterile operation.

The calibration of the flow sensor with different inks revealed a strong influence of the material on the measurements. The calibration curves for P30 and P25 could be fitted well ($R^2 = 0.9989$ and 0.9987) with an equation of the form $y = mx$, while A2L7 required an additional y-intercept ($y = mx + c$) which led to invalid measurement values at low

flow rates and has to be considered when assessing the validity of measurements.

3.2. Rheology

The rheological behavior of inks is one of the most relevant factors determining printability in extrusion-based bioprinting. The characteristics of the inks employed in this study were analyzed with oscillatory and rotational measurements. The storage and loss moduli (G' and G'') and the loss factor $tan\ \delta$ were determined in oscillatory measurements. Fig. 6 shows the performed amplitude sweeps in a range of 1–10 000 Pa. For all samples, the storage modulus G' was higher than the loss modulus G'' within the linear viscoelastic region, indicating a gel-like behavior for all investigated inks. The exact ratio of G' an G'' is expressed in the loss factor $tan\ \delta = G''/G'$ and was derived from the same measurements. The resulting values of $tan\ \delta$ are shown in Fig. 7, alongside the yield stress values determined in rotational measurements. Gel-like behavior is implied by $tan\ \delta < 1$ and lower values indicate a stronger dominance of elastic properties over viscous properties [26]. The lowest $tan\ \delta$ was found for P30 with 0.060 ± 0.006 and the highest for A2L7, but all samples were below $tan\ \delta = 0.17$ showing a strong dominance of elastic properties. The same trends are represented in the yield stress which was highest for P30 at (861 ± 32) Pa and lowest for A2L7 at (474 ± 5) Pa. A yield point could be detected for all inks. The results demonstrate the general suitability of the employed inks for bioprinting applications, as they all showed gel-like behavior ($tan\ \delta < 1$) and the presence of a yield point. High yield stress is an important factor determining printability [29], as it represents the ability of the ink to maintain its shape after extrusion.

3.3. Application of the adaptive pressure control

The performance of the presented setup for an adaptive PID pressure control was investigated employing three separate approaches. a) Continuous dispensing: To generally compare the resulting ink flow with and without adaptive pressure control, ink was continuously dispensed from a cartridge without printing any defined objects. The actual applicability of the setup in realistic scenarios was evaluated in two additional studies involving the printing of hollow cylinders as test objects. b) Adaptation to ink inhomogeneities: The ability to compensate for ink inhomogeneities by pressure adjustments was tested by printing from a cartridge with an intentionally inhomogeneous ink created by alternating layers of poloxamer 407 inks of different concentrations. c) Process transfer to other nozzle types: As an example for process transfer, the ability of the setup to adapt to nozzles with different lengths and geometries was investigated.

3.3.1. Continuous dispensing

The general capability of the real-time, adaptive pressure control to ensure a constant and reproducible ink flow was initially evaluated by simple, continuous dispensing runs. This approach allowed avoiding interference factors like pressure switching operations between printed layers. A separate ink-filled cartridge was used for each run and the ink was continuously dispensed for 30 min without printing any defined objects. Six runs were performed per ink, three with a constant pressure setting and three with the adaptive pressure control being active. Every run aimed at meeting a target flow of 300 µL/min. For the runs with adaptive pressure control, this could be achieved automatically without any preparatory work apart from the ink-specific flow sensor calibration to convert the sensor output to flow rate values. The continuous dispensing runs were then started with a pressure setting of 0 kPa and the pressure was automatically adapted by the PID control to an appropriate value within roughly 30 s. For the runs with constant pressure setting, a suitable pressure had to be determined first which was derived from the first adaptive run by averaging the applied pressure within a constant region over a period of 10 min. Flow measurements and pressure settings were recorded for the entire duration of each run.

Fig. 8 shows the recorded flow rate and pressure for P30 over time. A slightly smoothed flow rate is depicted in light blue and represents a rolling average over 15 data points, only including the valid data points as defined in section 2.3.2 (absolute value > 3 % of the sensor output limit and < 20 % change compared to the previous data point, also relative to the sensor output limit). The target flow rate is indicated in dark blue. The graphs A-C show the results of dispensing ink with a constant pressure setting, the graphs D-F represent the runs with

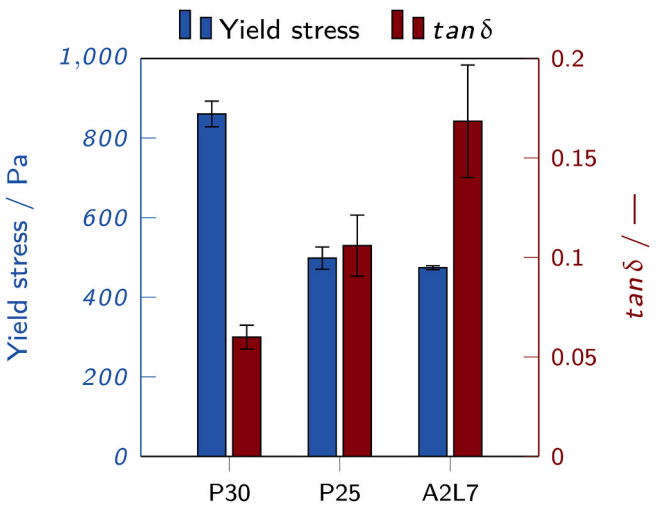

Fig. 7. Yield stress, as determined from rotational measurements, and loss factor $tan\ \delta$, as determined from oscillatory measurements, for all evaluated inks. The results show mean values ± standard deviation ($n = 3$).

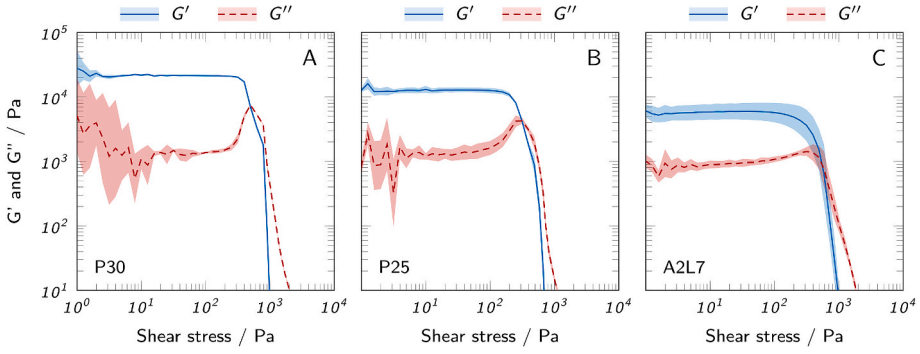

Fig. 6. Shear stress-controlled oscillatory measurements showing the storage modulus G' and loss modulus G'' for all prepared inks at an angular frequency of $\omega = 10$ s^{-1}. The results are depicted as mean values, the shaded areas represent the standard deviation ($n = 3$).

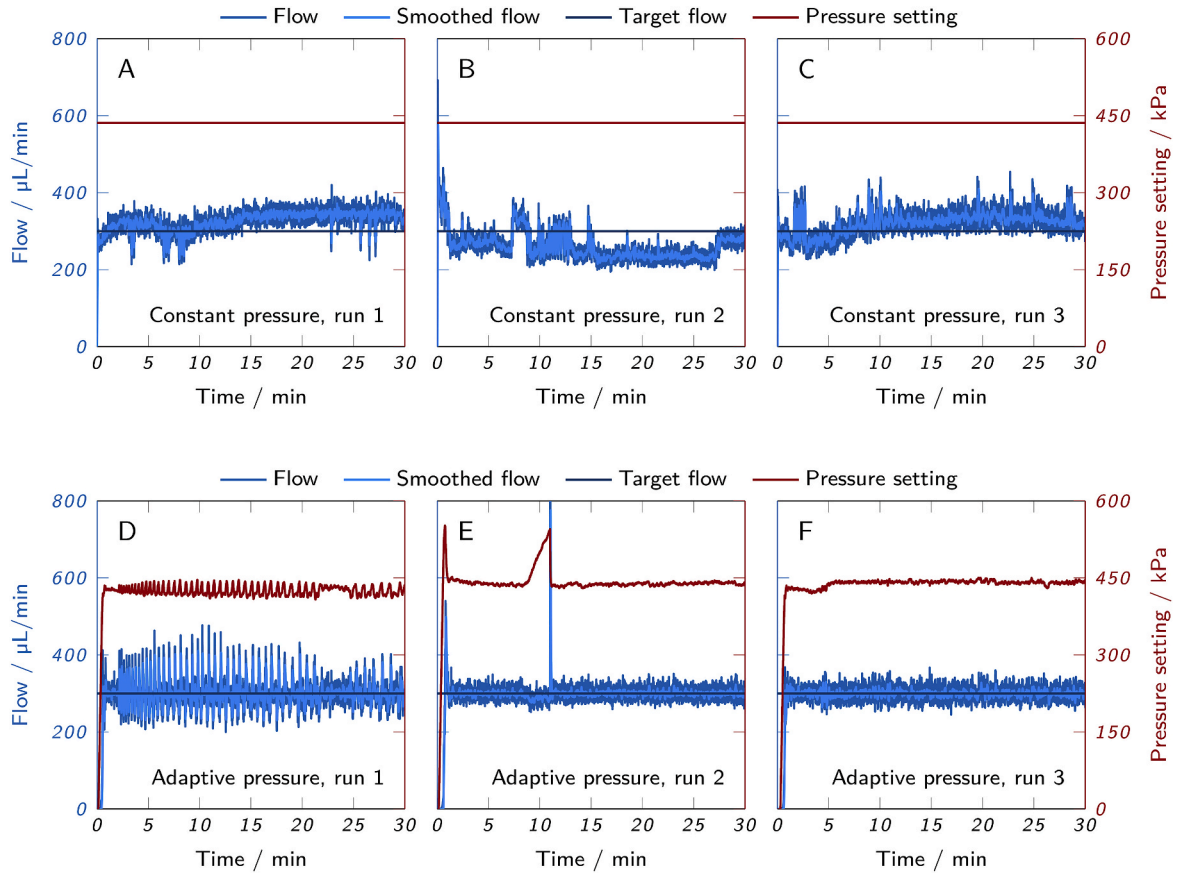

Fig. 8. Continuous dispensing runs of P30. The measured flow and the pressure setting are plotted over time. (A–C) Runs with constant pressure setting are compared to (D–F) runs with adaptive PID pressure control and a target flow rate of 300 µL/min.

adaptive pressure control.

A certain level of relatively uniform noise (roughly ±50 µL/min) was observed for the flow data of all runs, apparently a phenomenon that is inherent to the measurement method in combination with the investigated inks. It should be noted that the flow sensor is not designed for hydrogels or complex material compositions and showed considerably less noise in combination with water (data not shown). This implies that a large proportion of the observed noise can be attributed to the non-homogeneous nature of the inks containing micelles (P30 and P25) [57] or nanoclay and polymers (A2L7). A noticeably different noise pattern was observed for the first adaptive run with P30 (Fig. 8D), as the sensor noise was overlayed by additional fluctuations with higher amplitude and longer cycle length. These fluctuations also appeared in the recorded pressure settings indicating that they were not caused by measurement noise but by actual fluctuations of the applied pressure. The regularity of the fluctuations implies that the PID controller entered an oscillatory state, caused by repeatedly overshooting the desired set point and overcorrecting for it. This behavior can be counteracted by retuning the PID control loop, e. g. based on oscillatory characteristics or perturbation signals [58,59]. The mostly stable amplitude of the oscillations after 5 min implies a marginally stable system. For the second and third run of P30 with adaptive pressure control (Fig. 8E and F) and all runs with other inks, no oscillations occurred and the amount of noise corresponded to the runs with constant pressure setting, despite the same PID parameters being applied. As the oscillatory behavior was only observed in one of nine runs, it was not interpreted as an inherent issue of the employed setup. However, it revealed a potential pitfall when working with PID-controlled systems and a more systematic tuning of the PID parameters could increase the stability of the system [59].

Besides noise, additional irregularities on a larger timescale could be observed in the flow signal of the P30 runs with constant pressure setting (Fig. 8A–C). These irregularities did not follow a certain pattern, but seemed entirely erratic. A relatively similar behavior was observed for the first and third run. During the initial phase, the flow rate of both runs showed considerable variations that stabilized after 10–15 min at a flow rate of roughly 350 µL/min. Overall, the flow rate showed a slightly increasing trend and was mostly above the target flow. The second run showed erratic and sudden flow variations during the entire measurement, only with one relatively constant period between 15 min and 25 min where the flow was around 250 µL/min. Overall, the flow rate decreased during the run and was mostly below the target value. These results demonstrate that with regards to flow rate, both the consistency within a single run and the reproducibility between separate runs are limited when applying a constant pressure. Due to their erratic nature, no clear causes could be identified for the observed signal fluctuations and drifts. Potential influencing factors are ink inhomogeneities, temporary and partial nozzle clogging or manufacturing variations of cartridges and plugs [20,23]. The trends of increasing or decreasing flow rate suggest possible time-dependent parameters like temperature drifts or the cartridge fill level.

A very different behavior was observed for the runs with adaptive pressure control (Fig. 8D–F). Each run was started with a pressure setting of 0 kPa. The PID control was activated and performed the pressure adaptation automatically. The pressure was increased steadily, until the appropriate flow was achieved. This initial adaptation phase took roughly 30–60 s, before the pressure was stabilized at an appropriate level to generate a flow of 300 µL/min on average, corresponding to the desired target flow. For all three runs, the average flow was reliably kept constant for the whole duration of the measurement. However, as mentioned before, the first run showed considerable oscillations around the target value due to a suboptimal pressure regulation. In contrast, the second and third run achieved a similar amount of

noise as the runs with constant pressure. During the second run (Fig. 8E), a continuous pressure increase from roughly 440–540 kPa occurred between 9 min and 11 min, accompanied by a minor drop in flow rate. After 11 min, the flow rate suddenly jumped to the output limit of the sensor causing the pressure to drop quickly back to the base level. As a result, the flow rate also returned to the target value. Apparently, a partial clogging of the nozzle occurred here that was appropriately counteracted by the PID control by increasing the pressure, resulting in only a minor and short-term drop of flow rate. This demonstrates the suitability of the adaptive pressure control to compensate for unpredictable and erratic influencing factors like ink inhomogeneities or nozzle clogging and keep the flow at a constant rate.

For a more compact overview and simple comparison of different inks, all runs performed are depicted as swarm plots in Fig. 9. For P25 and A2L7, the corresponding plots of flow and pressure over time are shown in the supplementary material. Fig. 9 shows every performed run as a separate swarm of data points. The width of the swarm indicates the kernel density estimation, i. e. the number of data points at the corresponding flow rate. Additionally, all data points are plotted on a color map indicating the time point of the measurement. Thus, trends like a changing flow rate over the course of the measurement can be recognized in the form of color gradients.

The already discussed runs of P30 are shown in Fig. 9A. The first three swarms represent the runs with constant pressure, two of which are located largely above the target flow, while one is located below. The color gradients of the swarms indicate that each of these runs was accompanied by a steady change in flow rate implying a time-dependent influencing factor, as discussed before. The inconsistent positioning above and below the target flow demonstrates the lack of reproducibility and the limited capability to constantly meet the desired flow rate. By contrast, the swarms of the runs with an adaptive pressure setting are almost ideally centered around the target flow rate. The high fluctuations of the first run are reflected in the extended spread of the swarm along the y-axis.

Very similar observations could be made for the runs with P25 (Fig. 9B). While all runs with an adaptive pressure control met the target flow rate very accurately, this was only the case for the third run with constant pressure. The other runs were largely off the target flow, again indicating a lack of reproducibility. The noise of the measurements, represented by the extent of the swarms along the y-axis, was similar for all runs with adaptive pressure control and not larger than for the runs with constant pressure. No pressure oscillations due to inadequate PID tuning occurred.

Fig. 9C represents the measurements with A2L7. The comparison between runs with constant and adaptive pressure confirmed the previously made observations that the adaptive pressure control leads to an improved agreement between measured flow rate and target flow rate. The most noticeable difference of the A2L7 runs compared to P30 and P25 was the massively increased amount of noise across all runs. This behavior was also observed during the recording of calibration curves and seems to be inherent to the ink composition of A2L7. A systematic evaluation of noise behavior was not within the scope of this study. However, the stark contrast between the noise levels of the different inks implies that certain components typical for bioinks have a strong influence on the behavior and measurement quality of the flow sensor. While P30 and P25 only contain water and polymers, A2L7 has a more complex composition including solid nanoparticles. A systematic evaluation of the impact of different ink components and concentrations on the quality of the flow measurement should be the subject of future investigations. This investigation should also consider alternative types of flow sensors that might be better suited to provide accurate flow data for complex media like bioinks.

The continuous dispensing runs prove the suitability of the adaptive pressure control to rapidly generate a constant and defined ink flow, independent of the material and without the need for extensive parameter screenings. Adopting the flow rate as a relevant parameter in process development could simplify the transfer between different inks by aiming at a common target flow rate. Larger flow rate fluctuations could be shown to be reduced by the adaptive PID pressure control.

3.3.2. *Adaptation to ink inhomogeneities*

While continuous dispensing tests can provide valuable insights about the general behavior of the adaptive pressure control, they do not represent the intended application in 3D bioprinting. To investigate the capabilities of the adaptive pressure control more thoroughly in a realistic use case, simple 3D objects were printed from a cartridge with an intentionally inhomogeneous ink. The inhomogeneity was created by filling the cartridge with alternating layers of P30 and P25 to create a situation where the extrusion conditions change repeatedly over time due to the different rheological properties of both inks. For better visualization, the inks were dyed with food coloring, as depicted in Fig. 2B. To reduce the complexity of the printing process to a minimum, simple hollow cylinders were printed (10 mm diameter, 3 mm in height, 300 µm layers, 10 mm/s printing speed). For both runs, the sensor output was converted to flow rates based on the calibration curve of P30. A new cartridge containing three layers of P30 and three layers of P25 was used for each run.

Fig. 10 shows the initial phase of the two runs performed with constant and adaptive pressure side-by-side. Before starting a print with the adaptive pressure control, the pressure was set to zero and a continuous dispensing process was started to allow the PID control to gradually adapt the pressure, until a stable ink flow of 300 µL/min was achieved. This adaptation phase is represented in the first 45 s of Fig. 10B. The transitions from one printed layer to the next are clearly visible in the

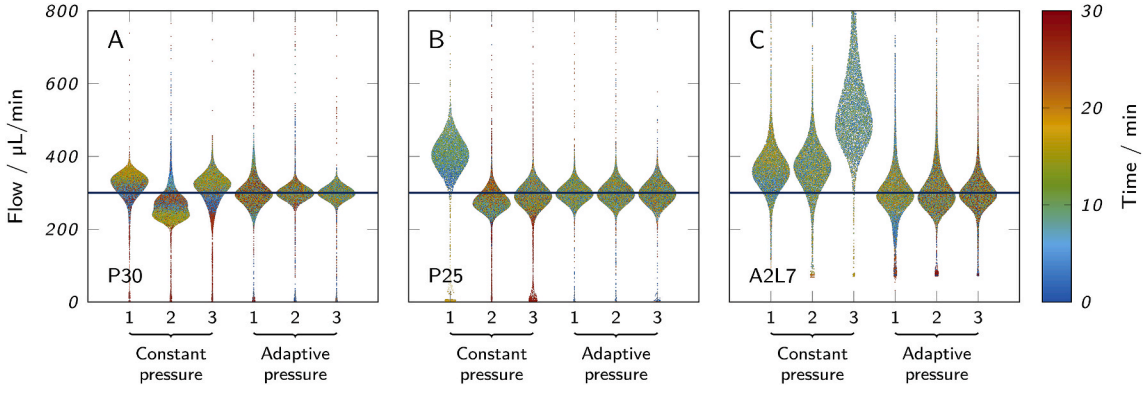

Fig. 9. Overview of all performed continuous dispensing runs depicted as swarm plots. Each swarm represents the first 30 min of a run performed with (A) P30, (B) P25 or (C) A2L7. The blue horizontal line indicates the target flow rate. (For interpretation of the references to color in this figure legend, the reader is referred to the Web version of this article.)

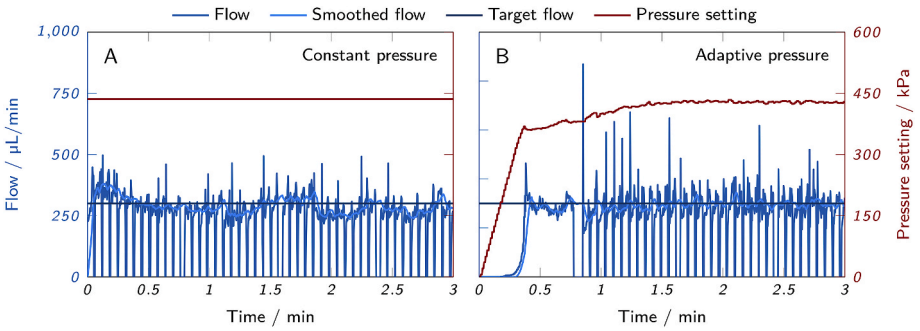

Fig. 10. Initial phase of hollow cylinder printing with an inhomogeneous ink. The graphs show flow rate and pressure setting over time for (A) a run with constant pressure and (B) a run with adaptive pressure control. With constant pressure, the printing process was started immediately. Adaptive runs were started with an initial adaptation phase of 30 s–60 s during which the pressure was adapted, until a constant ink flow was achieved.

form of sudden drops in flow rate, as the pressure is released from the cartridge during the transition and no ink is extruded. Particularly in the run with adaptive pressure, short spikes in flow rate occurred when the pressure was reapplied for the next layer. The PID control and the smoothed flow rate, depicted in the graphs light blue, were not affected by the flow rate drops and spikes, as they ignored invalid data points. All data points that were higher than 3% of the sensor output limit and changed less than 20% relative to the output limit compared to the previous data point were regarded as valid.

Fig. 11 presents the entire results of the two performed printing runs. Fig. 11A clearly visualizes the fluctuating flow rate when printing with a constant pressure setting optimized for P30. The measured flow rate was close to the target value of 300 µL/min at the beginning of the run when only P30 was extruded. The beginning extrusion of P25 after approximately 7–8 min was accompanied by a massive increase in flow rate. Thus, the three layers of P25 are reflected in the graph as three peaks of flow rate exceeding the output limit of the flow sensor. Between the layers, the flow rate did not return to the target value, but constantly exceeded it due to the mixing of the layers. As a result of the increased ink flow, the cartridge was already emptied after less than 23 min.

The PID control proved to be effective in compensating the rheologically different ink layers by continuously adapting the extrusion pressure. The three pressure peaks in Fig. 11B reflect the three layers of P30 which require a higher extrusion pressure than P25. The pressure minima of the same graph correspond to the layers of P25. The change in pressure was not sudden, but relatively gradual, indicating a certain degree of blending between the two inks. This effect is also manifested in the absolute values of the pressure maxima and minima that did not reach the same values as in the dispensing tests of the unblended inks. The frequent and relatively regular spikes in flow rate, especially observed in the run with adaptive pressure, were mainly caused by the sudden application of pressure to the cartridge at the start of a layer. They were accompanied by spikes of negative flow rate when the pressure was suddenly released again (not shown in the graph due to the cut-off at $y = 0$ µL/min). In general, these spikes were randomly observed in several printing runs and were not related to the PID control, but probably the presence of air bubbles in the cartridge. The available data are not sufficient to assess whether these spikes are negligible measurement artifacts or a real and significant effect with potential negative impacts on the printed objects.

The printed cylinders are shown in Fig. 11C and D. It is obvious that the cylinders printed with constant pressure exhibited a large range of different wall thicknesses due to the non-constant flow rate. Also, the cartridge was empty after only 28 cylinders, while 48 cylinders could be

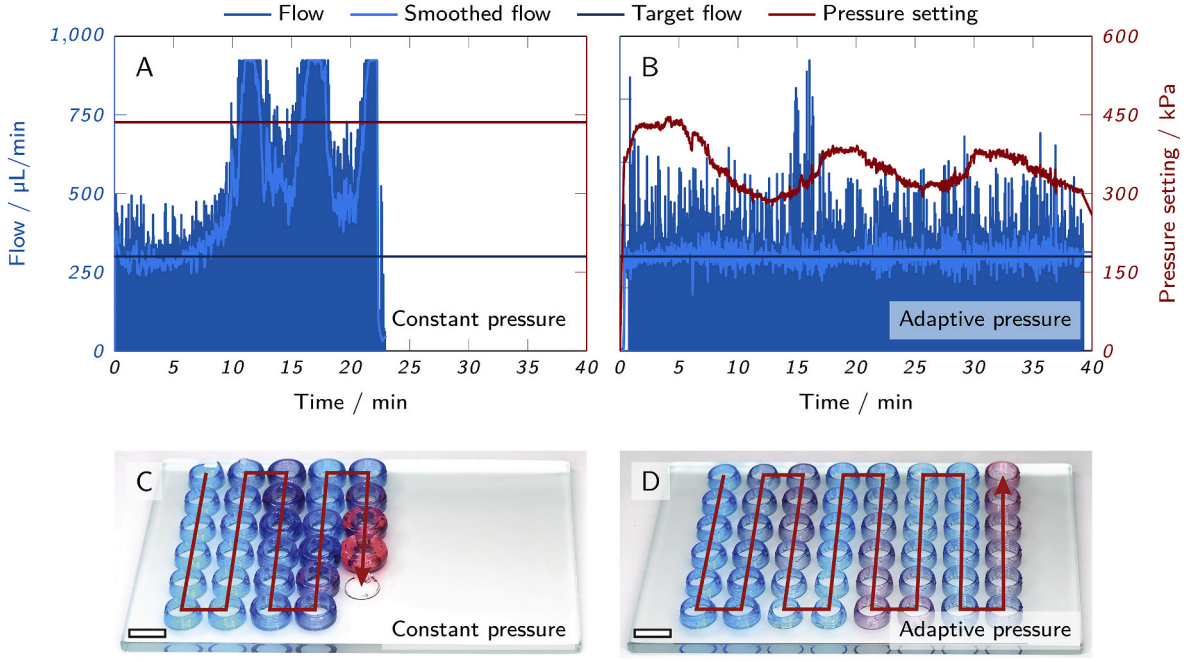

Fig. 11. Printing of hollow cylinders with an inhomogeneous ink. The graphs show flow rate and pressure setting over time, the photographs the printed cylinders of (A and C) a run with constant pressure and (B and D) a run with adaptive pressure control. The scale bars in (C) and (D) represent 10 mm.

printed with the adaptive pressure control without emptying the cartridge entirely. Here, the wall thicknesses of the cylinders were relatively constant, independent of the extruded ink, but slight deviations in the wall thicknesses could still be observed. This can partially be attributed to drying effects, as the whole printing process lasted for nearly 40 min, but another important contributor is the suboptimal calibration applied in this experiment. For every ink, a specific calibration curve was determined that allowed converting the sensor output data to flow rate values. In this case, the calibration curve of P30 was applied whose slope was about 12% higher than for P25 (see supplementary material). This resulted in a deviation between measured and real flow rate and caused a reduced ink flow when P25 was extruded.

The test prints with an inhomogeneous ink demonstrate the capability of the adaptive pressure control to perform real-time corrections of the extrusion pressure. The ink flow can be kept at a relatively constant value, even when conditions like ink viscosity vary over time due to inhomogeneities or environmental changes. Unlike the continuous dispensing, these experiments also demonstrate the applicability of the setup for printing and its potential profound impact on the resulting prints.

3.3.3. *Process transfer to other nozzle types*

Changing certain parameters in the experimental setup like nozzles, cartridges or printers usually requires adapting the extrusion pressure in order to achieve satisfactory printing results. Determining the appropriate pressure requires extensive parameter screenings and is often not done systematically based on objective criteria. Consequently, the process is susceptible to subjective, user-specific influences. To evaluate whether the adaptive pressure control based on flow measurements can facilitate process transfers from one experimental setup to another, printing runs were performed with different nozzles. Besides the rheological properties of the ink, the employed nozzle has the most substantial effect on the required pressure for printing. Due to different lengths, diameters and geometries (straight vs. tapered), the pressure drop along the nozzle can vary drastically. Here, the straight 1 inch nozzle employed in all other experiments was compared to another straight nozzle with a length of 1.5 inch and a tapered nozzle, as shown in Fig. 2C. All nozzles had the same orifice diameter of 0.58 mm. The underlying assumption of this experiment was that satisfactory printing results should be achievable with every nozzle, as long as the same flow rate of 300 µL/min is maintained. To examine the capability of the PID control to adapt to a new nozzle, four hollow cylinders were printed with each nozzle, two with a constant pressure setting, as determined for the 1 inch nozzle, and two with the adaptive pressure control being active. As before, the PID control was run for 30–60 s, until a relatively constant pressure was reached and the printing process could be started.

Fig. 12 shows an overview of all printed cylinders. With the 1 inch nozzle, there was hardly any difference between cylinders printed with constant pressure compared to the adaptive pressure control. For the 1.5 inch nozzle, there was an entirely different outcome. All cylinders printed with the adaptive pressure control looked virtually identical to the ones printed with the 1 inch nozzle. When applying the constant pressure setting optimized for the 1 inch nozzle, hardly any ink could be extruded, resulting in failed prints. The opposite effect was observed for the tapered nozzle. Here, the constant extrusion pressure caused an excessive amount of ink to be extruded which is why all prints were aborted after a single layer. In combination with the adaptive pressure control, intact cylinders could be printed with the tapered nozzle.

These results demonstrate the need to adjust the pressure for every nozzle separately. Typically, such adjustments are done manually and iteratively. The PID pressure control established here was shown to achieve this adjustment within a short time frame of 30–60 s and with a minimal loss of sample volume. Further improvements of time and material need are possible by systematically tuning the employed PID parameters. Regarding the change of nozzle types as a pars pro toto, it can be assumed that the adaptive pressure control also allows transfers to other experimental systems like different bioprinters. However, this would require basic process variables like printing speed, layer height and nozzle orifice diameter to remain unchanged.

3.4. *Potential challenges of working with complex cell-laden bioinks*

When working with cells or biological material, maintaining sterile conditions is an important aspect which can be accounted for by employing low-cost disposable sensors or autoclavable models. Wireless sensors may facilitate the handling in a biosafety cabinet. Considering the high sensitivity of cells, the sensor and connector design should be chosen carefully to minimize shear stress by avoiding sharp edges and using high-diameter capillaries.

Due to the commonly high cost of bioinks and cells, the potential loss of material should be considered in the design of sensors and connectors to minimize dead volumes. Optimizing the PID settings may contribute to minimizing the loss of material during the initial flow adaptation phase.

It should be considered that the addition of cells and the optimization of the biological functionality of inks may impair other ink properties like flow behavior, homogeneity, printability and the interaction with the flow sensor. As a result, limitations of the calibration range and differences in noise behavior and reproducibility have to be investigated in a material-specific approach. Within the scope of this paper, we already observed the influence of different additives at several concentrations on sensor noise and calibration range (see calibration curves in

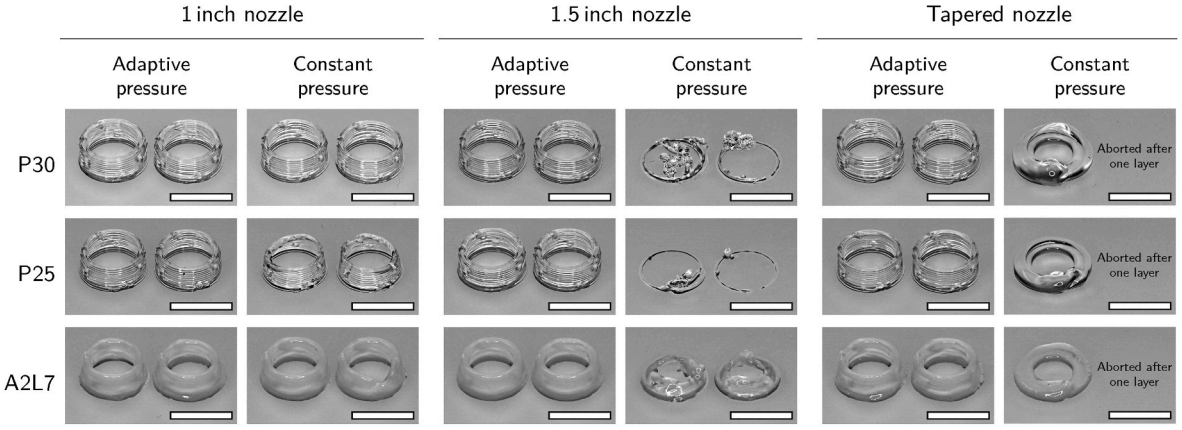

Fig. 12. Hollow cylinders printed with different inks and nozzles. The prints were performed with either a constant pressure optimized for a 1 inch straight nozzle or with adaptive pressure control after an adjustment phase of 30 s–60 s. The scale bars represent 10 mm.

the supplementary material). To assess the applicability of the presented flow control method for a wider range of complex bioinks, a systematic investigation about the influence of additives (e. g. nanoclay and polymers) and cells or special ink types (e. g. emulsions) on sensor performance is necessary. Incompatibilities with commercially available flow sensors may occur with certain types of bioinks that require more specialized equipment to guarantee printability. This includes thermosensitive bioinks, e. g. based on gelatin or agarose, that need to be extruded at a controlled temperature. Employing these inks in combination with the presented flow control would require either a controlled environment with constant temperature or a specialized flow sensor with an integrated temperature control.

3.5. Implications for process development, monitoring and control

Currently, process development for bioprinting applications often involves testing different settings for a range of parameters like pressure or printing speed. The results are assessed and suitable parameters chosen by the user in an iterative process. There is a range of approaches to find and provide objective and quantifiable criteria to determine suitable printing parameters. This includes mostly off-line analytics like evaluations of the fibre formation and rheological properties of inks [24] or filament collapse and fusion tests by image analysis [27]. Printability windows are often expressed as functions of extrusion pressure [24]. The presented application examples of the adaptive pressure control show an alternative approach based on flow rate as the leading parameter. When keeping certain parameters like nozzle orifice diameter, printing speed and layer height constant, processes can simply be transferred between different experimental systems, e. g. nozzle types or printers, by aiming at the same target flow rate. Transfers between different inks could be achieved with the same strategy, providing a material-independent approach. Adopting the flow rate as a material-independent, system--independent and user-independent parameter could lead to a paradigm shift in process development by allowing the definition of printability windows as a function of flow rate instead of pressure.

Flow rate measurements can also provide process monitoring data which are mostly not available in bioprinting. Often, there is no process monitoring at all or only qualitative monitoring, e. g. in the form of video recordings. Collecting data of the flow rate as an objective and quantifiable measurement parameter could support process validation and troubleshooting.

The main goal of the present study was to demonstrate the feasibility of an automatic adaptation of the extrusion pressure in real-time. Changes of extrusion conditions can occur when the viscosity of the extruded ink varies, e. g. due to inhomogeneities, time-dependent effects or shifting environmental conditions like temperature. Other factors like cartridge fill levels can alter extrusion conditions, as well. The performed case studies demonstrate the significant impact of actively and dynamically adapting the extrusion pressure to control the resulting ink flow. Thus, the PID-controlled setup provides a material-independent, system-independent and user-independent method to actively control and improve the printing process.

4. Conclusion

A PID-regulated pressure control for pneumatic extrusion-based bioprinting was established to monitor and control the flow rate of the dispensed ink. A Python-based software tool was implemented to process real-time data from a liquid flow meter and to continuously adapt the pressure in the bioprinter software to meet the specified target flow rate. The performance of the setup was evaluated with three different inks. A distinction was made between experiments with an active adaptive pressure control and experiments with a constant pressure setting. As use cases we investigated the following three scenarios: a) continuous dispensing, b) adaptation to ink inhomogeneities, c) process transfer to other nozzle types.

a) Continuous dispensing: Several runs of continuous dispensing demonstrated the successful automatic adjustment of pressure to consistently meet a specified target flow rate independently of the user. Compared to the constant pressure setting, the adaptive pressure control proved effective in compensating for environmental or system-related influences like nozzle clogging.
b) Adaptation to ink inhomogeneities: A more realistic use case was investigated by printing hollow cylinders from a cartridge filled with layers of two differently concentrated poloxamer 407 inks to simulate ink inhomogeneities. The adaptive pressure control proved effective in keeping a constant flow rate by adapting the pressure appropriately during the printing process. As a result, relatively consistent cylinders could be printed, whereas the constant pressure setting resulted in cylinders with strongly deviating wall thicknesses.
c) Process transfer to other nozzle types: To demonstrate the simple process transferability between different experimental setups, test prints were carried out with three different nozzle types with the same orifice diameter. The adaptive pressure control was able to generate the same constant flow rate with all three nozzle types within 30 s–60 s. The resulting cylinders were of consistent quality, independent of the nozzle. Prints with constant pressure setting suffered from a lack or abundance of extruded ink, if not performed with a pressure specifically determined for the corresponding nozzle type.

The presented PID-regulated adaptive pressure control proved effective in generating a specified target flow, compensating in real-time for varying extrusion conditions and adapting to changes of the experimental setup. The method provides a user-independent, material-independent and system-independent approach for process development, monitoring and control. A remaining challenge is the observed high noise level in the flow rate signal of the employed sensor depending on ink type. The employment or development of more suitable sensors for complex fluids like bioinks should be considered.

CRediT authorship contribution statement

Lukas Wenger: Conceptualization, Data curation, Investigation, Methodology, Software, Validation, Visualization, Writing – original draft. **Svenja Strauß:** Conceptualization, Data curation, Investigation, Methodology, Validation, Writing – original draft. **Jürgen Hubbuch:** Conceptualization, Writing – review & editing.

Declaration of competing interest

The authors declare that they have no known competing financial interests or personal relationships that could appear to influence the work reported in this paper.

Data availability

Data will be made available on request.

Acknowledgments

Funding: This work was supported by the German Federal Ministry of Education and Research (BMBF) as project SOP-Bioprint under contract number 13XP5071B. Furthermore, special thanks go to Bianca Schroth for her support.

Appendix A. Supplementary data

Supplementary data to this article can be found online at https://doi.org/10.1016/j.bprint.2022.e00229.

References

[1] I. Gibson, D. Rosen, B. Stucker, M. Khorasani, Additive Manufacturing Technologies, third ed., Springer, 2021 https://doi.org/10.2207/jjws.89.82.

[2] E. Kroll, D. Artzi, Enhancing aerospace engineering students' learning with 3D printing wind-tunnel models, Rapid Prototyp. J. 17 (5) (2011) 393–402, https://doi.org/10.1108/13552541111156522.

[3] B. Blakey-Milner, P. Gradl, G. Snedden, M. Brooks, J. Pitot, E. Lopez, M. Leary, F. Berto, A. du Plessis, Metal additive manufacturing in aerospace: a review, Mater. Des. 209 (2021), 110008, https://doi.org/10.1016/j.matdes.2021.110008.

[4] C. Parra-Cabrera, C. Achille, S. Kuhn, R. Ameloot, 3D printing in chemical engineering and catalytic technology: structured catalysts, mixers and reactors, Chem. Soc. Rev. 47 (1) (2018) 209–230, https://doi.org/10.1039/c7cs00631d.

[5] K.V. Wong, A. Hernandez, A review of additive manufacturing, ISRN Mech. Eng. (2012) 1–10, https://doi.org/10.5402/2012/208760, 2012.

[6] S.V. Murphy, A. Atala, 3D bioprinting of tissues and organs, Nat. Biotechnol. 32 (8) (2014) 773–785, https://doi.org/10.1038/nbt.2958.

[7] N.J. Castro, C. Meinert, P. Levett, D.W. Hutmacher, Current developments in multifunctional smart materials for 3D/4D bioprinting, Curr. Opin. Biomed. Eng. 2 (2017) 67–75, https://doi.org/10.1016/j.cobme.2017.04.002.

[8] B. Schmieg, J. Döbber, F. Kirschhöfer, M. Pohl, M. Franzreb, Advantages of hydrogel-based 3D-printed enzyme reactors and their limitations for biocatalysis, Front. Bioeng. Biotechnol. 6 (JAN) (2019) 1–12, https://doi.org/10.3389/fbioe.2018.00211.

[9] L. Wenger, C.P. Radtke, J. Göpper, M. Wörner, J. Hubbuch, 3D-Printable and enzymatically active composite materials based on hydrogel-filled high internal phase emulsions, Front. Bioeng. Biotechnol. 8 (2020) 1–17, https://doi.org/10.3389/fbioe.2020.00713.

[10] R. Langer, J.P. Vacanti, Tissue engineering, Science 260 (5110) (1993) 920–926.

[11] A.S. Hoffman, Hydrogels for biomedical applications, Adv. Drug Deliv. Rev. 64 (2012) 18–23, https://doi.org/10.1016/j.addr.2012.09.010, arXiv:NIHMS150003.

[12] S. Krishnamoorthi, A. Banerjee, A. Roychoudhury, Immobilized enzyme technology: potentiality and prospects, J. Enzymol. Metabol. 1 (1) (2015) 1–11.

[13] I.T. Ozbolat, M. Hospodiuk, Current advances and future perspectives in extrusion-based bioprinting, Biomaterials 76 (2016) 321–343, https://doi.org/10.1016/j.biomaterials.2015.10.076.

[14] J. Groll, J.A. Burdick, D.W. Cho, B. Derby, M. Gelinsky, S.C. Heilshorn, T. Jüngst, J. Malda, V.A. Mironov, K. Nakayama, A. Ovsianikov, W. Sun, S. Takeuchi, J. J. Yoo, T.B. Woodfield, A definition of bioinks and their distinction from biomaterial inks, Biofabrication 11 (1) (2018), https://doi.org/10.1088/1758-5090/aaec52.

[15] M. Hospodiuk, M. Dey, D. Sosnoski, I.T. Ozbolat, The bioink: a comprehensive review on bioprintable materials, Biotechnol. Adv. 35 (2) (2017) 217–239, https://doi.org/10.1016/j.biotechadv.2016.12.006.

[16] J. Malda, J. Visser, F.P. Melchels, T. Jüngst, W.E. Hennink, W.J.A. Dhert, J. Groll, D.W. Hutmacher, J. Malda, J. Visser, F.P. Melchels, W.J.A. Dhert, D.W. Hutmacher, 25th anniversary article: engineering hydrogels for biofabrication, Adv. Mater. 25 (36) (2013) 5011–5028, https://doi.org/10.1002/adma.201302042.

[17] C.P. Radtke, N. Hillebrandt, J. Hubbuch, The Biomaker: an entry-level bioprinting device for biotechnological applications, J. Chem. Technol. Biotechnol. 93 (3) (2018) 792–799, https://doi.org/10.1002/jctb.5429.

[18] L.R. Darwish, M.T. El-Wakad, M.M. Farag, Towards an ultra-affordable three-dimensional bioprinter: a heated inductive-enabled syringe pump extrusion multifunction module for open-source fused deposition modeling three-dimensional printers, J. Manuf. Sci. Eng. 143 (12) (2021), https://doi.org/10.1115/1.4050824.

[19] D. Bociaga, M. Bartniak, K. Sobczak, K. Rosinska, An integration of a peristaltic pump-based extruder into a 3D bioprinter dedicated to hydrogels, Materials 13 (19) (2020), https://doi.org/10.3390/MA13194237.

[20] P. Fisch, M. Holub, M. Zenobi-Wong, Improved accuracy and precision of bioprinting through progressive cavity pump-controlled extrusion, Biofabrication 13 (2021) 1–18, https://doi.org/10.1101/2020.01.23.915868, 2021.

[21] L. Ning, B. Yang, F. Mohabatpour, N. Betancourt, M.D. Sarker, P. Papagerakis, X. Chen, Process-induced cell damage: pneumatic versus screw-driven bioprinting, Biofabrication 12 (2) (2019), https://doi.org/10.1088/1758-5090/ab5f53.

[22] K. Hölzl, S. Lin, L. Tytgat, S. Van Vlierberghe, L. Gu, A. Ovsianikov, Bioink properties before, during and after 3D bioprinting, Biofabrication 8 (3) (2016) 1–19, https://doi.org/10.1088/1758-5090/8/3/032002.

[23] S. Seiffert, J. Sprakel, Physical chemistry of supramolecular polymer networks, Chem. Soc. Rev. 41 (2) (2012) 909–930, https://doi.org/10.1039/c1cs15191f.

[24] N. Paxton, W. Smolan, T. Böck, F. Melchels, J. Groll, T. Jungst, Proposal to assess printability of bioinks for extrusion-based bioprinting and evaluation of rheological properties governing bioprintability, Biofabrication 9 (4) (2017), 44107, https://doi.org/10.1088/1758-5090/aa8dd8.

[25] Y. Zhao, Y. Li, S. Mao, W. Sun, R. Yao, The influence of printing parameters on cell survival rate and printability in microextrusion-based 3D cell printing technology, Biofabrication 7 (4) (2015), https://doi.org/10.1088/1758-5090/7/4/045002.

[26] T.G. Mezger, The Rheology Handbook, fourth ed., Vincentz Network GmbH & Co. KG, Hanover, 2014.

[27] A. Ribeiro, M.M. Blokzijl, R. Levato, C.W. Visser, M. Castilho, W.E. Hennink, T. Vermonden, J. Malda, Assessing bioink shape fidelity to aid material development in 3D bioprinting, Biofabrication 10 (1) (2017), https://doi.org/10.1088/1758-5090/aa90e2.

[28] N. Soltan, L. Ning, F. Mohabatpour, P. Papagerakis, X. Chen, Printability and cell viability in bioprinting alginate dialdehyde-gelatin scaffolds, ACS Biomater. Sci. Eng. 5 (6) (2019) 2976–2987, https://doi.org/10.1021/acsbiomaterials.9b00167.

[29] V.H.M. Mouser, F.P.W. Melchels, J. Visser, W.J.A. Dhert, D. Gawlitta, J. Malda, Yield stress determines bioprintability of hydrogels based on gelatin-methacryloyl and gellan gum for cartilage bioprinting, Biofabrication 8 (3) (2016), 035003, https://doi.org/10.1088/1758-5090/8/3/035003.

[30] B. Webb, B.J. Doyle, Parameter optimization for 3D bioprinting of hydrogels, Bioprinting 8 (July) (2017) 8–12, https://doi.org/10.1016/j.bprint.2017.09.001.

[31] M. Matamoros, J.C. Gómez-Blanco, Á.J. Sánchez, E. Mancha, A.C. Marcos, J. P. Carrasco-Amador, J.B. Pagador, Temperature and humidity PID controller for a bioprinter atmospheric enclosure system, Micromachines 11 (11) (2020), https://doi.org/10.3390/mi11110999.

[32] R. Opel, W.R. Hynes, M. Moya, Flow Sensor Integration for Precision Dispensing of Visco-Elastic Biomaterials, 2017.

[33] S. Strauß, B. Schroth, J. Hubbuch, Evaluation of the reproducibility and robustness of extrusion-based bioprinting processes applying a flow sensor, Front. Bioeng. Biotechnol. 10 (2022) 1–14, https://doi.org/10.3389/fbioe.2022.831350.

[34] W.J. Fleming, Overview of automotive sensors, IEEE Sensor. J. 1 (4) (2001) 296–308.

[35] U. Schmid, G. Krötz, D. Schmitt-Landsiedel, A volumetric flow sensor for automotive injection systems, J. Micromech. Microeng. 18 (4) (2008), https://doi.org/10.1088/0960-1317/18/4/045006.

[36] Y. Li, W. Yang, C. G. Xie, S. Huang, Z. Wu, D. Tsamakis, C. Lenn, Gas/oil/water flow measurement by electrical capacitance tomography, Meas. Sci. Technol. 24 (7). doi:10.1088/0957-0233/24/7/074001.

[37] R. Thorn, G. A. Johansen, B. T. Hjertaker, Three-phase flow measurement in the petroleum industry, Meas. Sci. Technol. 24 (1). doi:10.1088/0957-0233/24/1/012003.

[38] D.L. Polla, A.G. Erdman, W.P. Robbins, D.T. Markus, J. Diaz-diaz, R. Rizq, Y. Nam, H.T. Brickner, A. Wang, P. Krulevitch, Microdevices in medicine, Annu. Rev. Biomed. Eng. 2 (1) (2000) 551–576, https://doi.org/10.1146/annurev.bioeng.2.1.551.

[39] C.J. Okereke, O.A. Lasode, I.O. Ohijeagbon, Exergoeconomic analysis of an industrial beverage mixer system: process data, Data Brief 32 (2020), 106125, https://doi.org/10.1016/j.dib.2020.106125.

[40] L.D. Pedersen, Assessment of sensors used in the food industry, Food Control 2 (2) (1991) 87–98, https://doi.org/10.1016/0956-7135(91)90144-L.

[41] N.T. Nguyen, Micromachined flow sensors - a review, Flow Meas. Instrum. 8 (1) (1997) 7–16, https://doi.org/10.1016/S0955-5986(97)00019-8.

[42] J.T. Kuo, L. Yu, E. Meng, Micromachined thermal flow sensors - a review, Micromachines 3 (3) (2012) 550–573, https://doi.org/10.3390/mi3030550.

[43] S. Silvestri, E. Schena, Micromachined flow sensors in biomedical applications, Micromachines 3 (2) (2012) 225–243, https://doi.org/10.3390/mi3020225.

[44] C. Li, P.M. Wu, J.A. Hartings, Z. Wu, C.H. Ahn, D. Ledoux, L.A. Shutter, R. K. Narayan, Smart catheter flow sensor for real-time continuous regional cerebral blood flow monitoring, Appl. Phys. Lett. 99 (23) (2011) 10–14, https://doi.org/10.1063/1.3669705.

[45] G. Dumortier, J.L. Grossiord, F. Agnely, J.C. Chaumeil, A review of poloxamer 407 pharmaceutical and pharmacological characteristics, Pharmaceut. Res. 23 (12) (2006) 2709–2728, https://doi.org/10.1007/s11095-006-9104-4.

[46] J.A. Rowley, G. Madlambayan, D.J. Mooney, Alginate hydrogels as synthetic extracellular matrix materials, Biomaterials 20 (1) (1999) 45–53, https://doi.org/10.1016/S0142-9612(98)00107-0.

[47] A.D. Augst, H.J. Kong, D.J. Mooney, Alginate hydrogels as biomaterials, Macromol. Biosci. 6 (8) (2006) 623–633, https://doi.org/10.1002/mabi.200600069.

[48] F. Pahlevanzadeh, H. Mokhtari, H.R. Bakhsheshi-Rad, R. Emadi, M. Kharaziha, A. Valiani, S.A. Poursamar, A.F. Ismail, S. RamaKrishna, F. Berto, Recent trends in three-dimensional bioinks based on alginate for biomedical applications, Materials 13 (18) (2020) 3980, https://doi.org/10.3390/ma13183980.

[49] S. Duin, K. Schütz, T. Ahlfeld, S. Lehmann, A. Lode, B. Ludwig, M. Gelinsky, 3D bioprinting of functional islets of langerhans in an alginate/methylcellulose hydrogel blend, Adv. Healthcare Mater. 8 (7) (2019) 1–14, https://doi.org/10.1002/adhm.201801631.

[50] F.F. Cai, S. Heid, A.R. Boccaccini, Potential of Laponite® Incorporated Oxidized Alginate-Gelatin (ADA-GEL) Composite Hydrogels for Extrusion-Based 3D Printing, 2021, https://doi.org/10.1002/jbm.b.34771.

[51] M. Shen, Y. Sun, J. Xu, X. Guo, R.K. Prud'Homme, Rheology and adhesion of poly (acrylic acid)/laponite nanocomposite hydrogels as biocompatible adhesives, Langmuir 30 (6) (2014) 1636–1642, https://doi.org/10.1021/la4045623.

[52] G. Schnell, R. Schäfer, Ein thermischer Durchflußsensor für die Infusionstechnik, Biomed. Tech. 40 (3) (1995) 50–53, https://doi.org/10.1515/bmte.1995.40.3.50.

[53] Sensirion, STEP File Sensirion SLI, Sensirion, 2021. URL, https://sensirion.com/resource/cad/sli.

[54] V. Dubey, H. Goud, P.C. Sharma, Role of PID control techniques in process control system: a review, in: P. Nanda, V.K. Verma, S. Srivastava, R.K. Gupta, A. P. Mazumdar (Eds.), Data Engineering for Smart Systems, Springer, Singapore, 2022, pp. 659–670.

[55] R.A. Paz, PhD. thesis, The Design of the PID Controller, Klipsch School of Electrical and Computer Engineering, 2001.

[56] G. Wolterink, A. Umrani, M. Schouten, R. Sanders, G. Krijnen, 3D-Printed Calorimetric Flow Sensor, 2020, IEEE Sensors, 2020, pp. 1–4, https://doi.org/10.1109/SENSORS47125.2020.9278640.

[57] I.R. Schmolka, Physical basis for poloxamer interactions, Ann. N. Y. Acad. Sci. 720 (1) (1994) 92–97, https://doi.org/10.1111/j.1749-6632.1994.tb30437.x.
[58] H. Seki, T. Shigemasa, Retuning oscillatory PID control loops based on plant operation data, J. Process Control 20 (2) (2010) 217–227, https://doi.org/10.1016/j.jprocont.2009.12.004.
[59] H.O. Bansal, R. Sharma, P.R. Shreeraman, PID controller tuning techniques: a review, J. Control Eng. Technol. 2 (4) (2012) 168–176.